FAN SIMILARITY MODEL FOR THE FAN-INTAKE INTERACTION PROBLEM

Mauro Carnevale
Osney Thermo-Fluids Laboratory
Department of Engineering Science,
University of Oxford,
Oxford OX2 0ES, UK
e-mail: mauro.carnevale@eng.ox.ac.uk

Feng Wang
Osney Thermo-Fluids Laboratory
Department of Engineering Science,
University of Oxford,
Oxford OX2 0ES, UK
e-mail: feng.wang@eng.ox.ac.uk

Anthony B. Parry
Rolls-Royce plc
Derby, UK
e-mail: anthony.parry@rolls-royce.com

Jeffrey S. Green
Rolls-Royce plc
Derby, UK
e-mail: jeff.green@Rolls-Royce.com

Luca di Mare
Osney Thermo-Fluids Laboratory
Department of Engineering Science,
University of Oxford,
Oxford OX2 0ES, UK
e-mail: luca.dimare@eng.ox.ac.uk

ABSTRACT

Very high-bypass ratio turbofans with large fan tip diameter are an effective way of improving the propulsive efficiency of civil aero-engines. Such engines, however, require larger and heavier nacelles, which partially offset any gains in specific fuel consumptions. This drawback can be mitigated by adopting thinner walls for the nacelle and by shortening the intake section. This binds the success of very high-bypass ratio technologies to the problem of designing an intake with thin lips and short diffuser section which is well matched to a low speed fan. Consequently the prediction of the mutual influence between the fan and the intake flow represents a crucial step in the design process.

Considerable effort has been devoted in recent years to the study of models for the effects of the fan on the lip stall characteristics and the operability of the whole installation. The study of such models is motivated by the wish to avoid the costs incurred by full, three-dimensional CFD computations. The present contribution documents a fan model for fan-intake computations based on the solution of the double linearization problem for unsteady, transonic flow past a cascade of aerofoils with finite mean load. The computation of the flow in the intake is reduced to a steady problem, whereas the computation of the flow in the fan is reduced to one steady problem and a set of solutions of the linearised model in the frequency domain. The nature of the approximations introduced in the fan representation is such that numerical solutions can be computed inexpensively, whilst the main feature of the flow in the fan passage, namely the shock system and an approximation of the unsteady flow encountered by the fan are retained. The model is applied to a well-documented test case and compares favourably with much more expensive three-dimensional, time domain computations.

1 INTRODUCTION

Current regulations in aviation are motivated by the necessity of balancing the economic benefits of air travel with its impact on the environment and local communities. The consequent legislation requires the introduction of engines with reduced specific fuel

consumption (SFC) on commercial aircraft. An effective way of lowering SFC is an improvement in propulsive efficiency. This can be achieved by increasing the bypass ratio and lowering the fan pressure ratio and tip Mach number. An increase in engine diameter also entails a potential increase in nacelle weight and size. In turn, a larger and heavier nacelle can obliterate any gain in performance due to a higher bypass ratio; Peters et al. [1] pointed out that a 1% reduction in nacelle weight corresponds in a 0.07% increase in propulsive efficiency. Therefore it is necessary to design nacelles with shorter and thinner lips in order to reduce the weight and drag of the installation for any further rise in bypass ratio to be truly advantageous. Thinner intake lips and shorter diffuser sections exacerbate the adverse pressure gradients acting on the intake flow during operations at incidence or cross wind and increase the risk of conveying a highly distorted flow to the fan face. This can result in a reduction in the stable operating range of the fan and potentially affects the mechanical integrity of the blades. The fan, in turn, is known to affect the flow in the intake, generally increasing the lip stall-free range of operation, as shown by Hodder [2].

The interaction between the fan and the intake flow, and the beneficial effect of the fan on the lip stall characteristics of the intake have been widely investigated experimentally. Hodder [2] first tried to separate the effects of Reynolds number and engine interaction. Larking and Schweinger [3] quantified the beneficial effect of the fan by increasing the lip stall-free range of the intake by about 3 or 4 degrees incidence. They also demonstrated methods to simulate the effect of the fan in an intake rig without recourse to rotating turbomachinery. Boldman et al. [4] demonstrated the beneficial effect of the presence of the fan in postponing the angle at which the lip stall up to 7 degrees with respect to the isolated intake. In this work they demonstrated that this effect depends on the mass flow rate and, consequently, from the Mach number at fan face.

A number of numerical studies on the fan-intake interaction problem are also available in literature. Recently Carnevale et al. [5] carried out a computational investigation focused on separation occurrence in a subsonic civil aircraft flying at incidence. Their study has investigated the interaction between the separation and the fan stage. They pointed out the relation between the distortion affecting the fan and the potential effect due to the LPC system presence. Cao et al. [6] performed an extensive analysis of a short-intake at high incidence. Consistent with previous experimental investigations, both studies demonstrated by means of steady RANS and Unsteady RANS (URANS) the beneficial effect of the presence of the fan. This effect is due to the mechanism of redistribution of the flows in the intake region. A common feature of numerical studies based on URANS simulations is the high computational cost. The factors leading to high computational demands are the spatial resolution requirements in the fan set and the time step limitations, which are bound to the fan blade passing frequency. The spatial resolution requirements in the fan are such that in a typical URANS fan-intake calculation, about 80% of the grid points are in the fan domain.

The high cost of URANS-based models has generated growing interest in approximate models for the fan-intake interaction problem. The basic ingredient of the fan-intake interaction problem is the ability of the fan to modify the static pressure field in the intake and hence to redistribute the flow in the intake. In the presence of a distorted inlet, the part of the fan admitting air of lower axial velocity operates a higher static pressure rise because the relative exit flow angle is fixed by the Kutta condition. If the exit static pressure is uniform, then the static pressure at the fan face is lowered in correspondence with those areas of low inlet axial velocity, thereby modifying the axial pressure gradient in the intake duct. The action of the fan allows the intake to operate in a stall-free regime even at incidence angles corresponding to stalled flow for the intake without fan. The basic ingredients of this interaction are present in an actuator disc model (see Hawthorne [7] and Kaji et.al. [8]). Hynes [9] developed such a model and coupled it to a three-dimensional numerical model for the intake. Longley [10] further refined the model by including the effect of the inertia of the fluid in the fan passages. This was achieved by a series of one-dimensional channels connected to a three-dimensional CFD computation of the intake.

A now popular alternative to the actuator disc model is the body force model. The body force model tries to approximate the action of the fan by a field of body forces that give the same change in angular momentum and entropy as the fan as shown in Marble [11]. This approach can be implemented easily by adding appropriate source terms in to the RANS equations rather than meshing the fan set, which allows a drastic reduction in the overall computational costs. Gong [12] implemented an analytical body force model for stall inception in high-speed compressors. This work has represented the starting point for a large number of improved models such as the work of Defoe et al. [13], who introduce perturbations to generate shocks in the passage, and Thollet et al. [14], who improved the calibration procedure in the Gong's model and applied it to investigate the fan-intake interaction. Recently, Cao et al. [15] implemented a body force model based on the idea of gradually turning flow along the fan camber line. The model was validated on rotor 67.

Among the low fidelity model a further alternative to CFD is represented by the frequency domain approaches. Pullan and Adamczyk [16] proposed a new procedure based on the filtering of high frequencies through a modified mixing plane with the aim of decreasing the computational costs in CFD. He and Ning [17] and Hall et al. [18] developed frequency domain methods for low reduced frequency problems. A more exhaustive review of these methods can be found in He [19]. Frequency domain methods are based on a-priori knowledge of the frequencies appearing in the spectrum the flow quantities. Fan-intake interaction problems fall within this set of flows. Furthermore, Carnevale et al. [20] analysed the behaviour of the fan in response to low frequency distortions and found that the response is dominated by low-frequency, long-wavelength disturbances and that a linearised response model is adequate to reproduce the flow

patterns observed in time-domain, unsteady calculations.

A novel similarity model for fan-intake interaction problems is presented in this paper. The model relies on reasonable assumptions about the harmonic content of the disturbances entering the fan set and on the flow pattern in the fan passage. The model does not require any calibration procedure and it is able to predict the perturbation response of the fan to the low frequency distortions. Furthermore, the model computes approximate unsteady pressure fields on the fan surfaces for use in forced response calculations. For the purpose of computing the effect of the fan on the intake flow, the model is coupled with a steady CFD approach. The effect of the fan coupled to an intake operating at incidence is computed and the results compared with the URANS results in Carnevale et al. [20].

2 CASE STUDY

The case study chosen for this paper is representative of a subsonic intake for commercial service. The general arrangement of the flow in flight at incidence with stalled lip is shown in Figure 1. The flow goes above the stagnation point (A) on the lower surface of the nacelle, and turns sharply around the lower lip (B). The strong acceleration caused by the small radius of curvature of the lip may cause the flow to re-laminarize. Furthermore, at high enough flight Mach numbers, the flow will cross sonic conditions and will decelerate through a normal shock (C). Even in the absence of a shock, the change in curvature of the wall is accompanied by an adverse pressure gradient which, at high enough incidence, will cause the flow to separate (E). The separation brings with it vorticity and distortion affecting the fan and the downstream region (D).

The parameters affecting the flow pattern are the Reynolds number, the Mach number (or equivalently the mass flow rate through the intake), and the flow incidence. Flow separation at the lower lip of the intakes results in high total pressure distortions which reduce fan stall margin and induce forced vibrations in the fan blade. The incidence at which large separations appear in the intake duct, therefore, determines the operability limit of the aircraft.

The scenario just described without the presence of the rotating fan is generally known as aspirated configuration. An intake coupled with the rotating fan stage is defined as powered intake.

3 METHODOLOGY

As discussed in the previous sections, the effect of the fan on the intake flow is a consequence of the static pressure rise and exit flow angle characteristics of the fan. These characteristics can be reproduced by simple models and the largest savings in computational effort for a typical URANS calculation are to be obtained in the fan domain. Therefore it is natural to seek an approximate treatment for the flow in the fan passages.

3.1 The similarity model for the fan

The derivation of the model presented in this paper starts from the Euler equations. The flow in the fan passages is assumed to be inviscid and approximations are sought which make certain details of the geometry superfluous, e.g. the curvature radii of the leading and trailing edge, and allow numerical solutions to be obtained inexpensively. The derivation is illustrated for clarity in two-space dimensions, but the extension to three space dimensions is straightforward.

The similarity model (S.M.) contained in the present derivation is based on the assumption that the streamlines in the fan passage deviate little from the direction of the camber line of the fan. With reference to Figure 2 and handling a two-dimensional case for simplicity, let ξ and η be curvilinear coordinates in the direction of the nominal streamline (i.e. the camber line) and the direction normal to it. Let ξ also be a small parameter and let the velocity components in the direction be of order $\mathcal{O}(\varepsilon_1)$. The Euler equation can now be written in conservation form as

$$0 = -\frac{\partial S}{\partial \xi} - \frac{\partial T}{\partial \eta} \tag{1}$$

The vectors S and T are the fluxes of the conserved variables

$$S = \rho \begin{bmatrix} u^{\xi} \\ u^{\ell} u_{[j\ell,\xi]} \\ u^{\ell} u_{[j\ell,\eta]} \\ u^{\xi} h \end{bmatrix} + \begin{bmatrix} 0 \\ m^{\xi} \\ m^{\eta} \\ 0 \end{bmatrix} p \tag{2}$$

$$T = \rho \begin{bmatrix} u^{\eta} \\ u^{\ell} u_{[j\ell,\xi]} \\ u^{\ell} u_{[j\ell,\eta]} \\ u^{\eta} h \end{bmatrix} + \begin{bmatrix} 0 \\ n^{\xi} \\ n^{\eta} \\ 0 \end{bmatrix} p \tag{3}$$

where u_{ξ} and u_{η} are the covariant velocity components and u^{ξ} and u^{η} are the contravariant velocity components and m^{ξ},m^{η} and n^{ξ} and n^{η} are the components of the contravariant metric tensor. The terms $u^{\ell} u_{[j\ell,\xi]}$ and $u^{\ell} u_{[j\ell,\eta]}$ include the definition of the Christofell symbol, which take in account the deviation of the streamline from the straight line direction. The convection adopted is the same adopted to Aris [21]. The small perturbation approximation is now introduced requiring

$$\frac{u_{\eta}}{u_{\xi}} = \varepsilon_1 \ll 1 \tag{4}$$

The similarity parameter ε_1 is proportional to the blade thickness δ or, more precisely, to its derivative with respect to the curvilinear coordinate ξ (see Figure 2).

$$u^{\eta} = u_{\xi} \frac{d\delta}{d\xi} = \varepsilon_1 u_{\xi} \tag{5}$$

Simplifications can be introduced in equations (1-3) by neglecting terms of order $\mathscr{O}(\varepsilon_1^2)$. The effect of these approximations is to remove the contribution of the η-wise velocity component from the total enthalpy and to remove the contribution of the normal momentum flux in the η-direction.

This features of the model weakens the coupling between the stream-wise and normal velocity and give rise to a $\sqrt{\varepsilon_1}$ scaling of the gradient in the η-direction.

When the fan passage operate in distorted flow generated by the intake, the flow in the fan is unsteady. The time variation of the flow can be represented as Fourier series

$$U(\xi,\eta,t) = U(\xi,\eta) + \sum_{k=1}^{N_k} \varepsilon_k \widehat{U}_k(\xi,\eta) e^{ik\Omega} \tag{6}$$

Where N_k is sufficient large integer number. The complex amplitudes $\widehat{U}(\xi,\eta)$ can be determined solving the linearized problem

$$ik\Omega\widehat{U}_k = -\frac{\partial}{\partial\xi}\left(\frac{\partial S}{\partial U}\widehat{U}_k\right) - \frac{\partial}{\partial\eta}\left(\frac{\partial T}{\partial U}\widehat{U}_k\right) \tag{7}$$

For the purpose of numerical solution, the blade passage can be approximated with a simple Cartesian $H-$grid in the (ξ,η) plane and the fluxes S, T, $\widehat{S}_k$ and $\widehat{T}_k$ can be treated as split fluxes, e.g. using Van Leer-Hanel flux vector splitting. Symbolic differentiation of the routines used to compute the fluxes and yields the routines to compute the perturbation fluxes $\widehat{S}_k$ and $\widehat{T}_k$. The set of Equations (1-3), Equation 6, and equation7, including the approximation in Equation (4) can be discretized using Bubnov-Galerkin methods.

For high-stagger cascades the η-direction is far from the direction of the cascade plane. This means that gradients in the η-direction cannot be evaluated accurately using standard finite difference formulation because numerical gradients contain contributions from both the η and ξ the directions, but these this limitation, the discretization used in this paper uses a Cartesian grid in η,ξ plane. Fluxes have been calculated by assuming two sets of degrees of freedom are attributed to each cell, so that gradients in the η-direction can be evaluated along lines almost orthogonal to the ξ-lines. This procedure is usually defined to pseudo-Galerkin (P-G) approach.

3.2 Coupling procedure: RANS + S.M.

For the purpose of computing fan-intake interaction problems, the fan model is therefore composed of the time-mean model and N_k frequency domain linearized models coupled to a steady state RANS model of the intake. The frequency domain model is linearized around the time-mean solution computed by model according the equation (1). The boundary conditions for the fan models are obtained performing Fourier transforms of the flow field at fan face, as computed by the intake flow solution. The intake solution, conversely, uses the flow field at the fan face reconstructed by composing the mean solution and the contribution from the linearization of the solution including N_k harmonics. When presenting data to the intake domain, the components of the signal representing moving disturbances in the intake frame of reference are filtered out.

3.3 Coupling procedure: URANS + URANS

For the purpose of validation, the model presented in the previous section is applied to a fan-interaction problem on a well-documented test case, previously studied by Carnevale et al. [20]. The interaction between the fan and the intake, as predicted by the present method, is compared to fully three- dimensional, time domain URANS simulations. Data for the aspirated intake case are also shown. The aspirated intake results are based on RANS calculation due to the symmetry of the problem. The mesh consists of approximately 2×10^7 elements. The grid convergence study and more detailed results is provided in Carnevale et al. [20]. The steady calculations are used as initial state of the for the URANS calculations in the intake-fan coupled simulations. For URANS calculations, the whole annulus fan domain is discretized with 2×10^7 elements. The mesh is obtained by meshing one fan passage in Figure 3-b and replicating it around the annulus. All the meshes have been created with an in-house mesh generator descritebed by Wang et al in [22] and [23].

3.4 Computational costs

The two coupling procedures described imply a great difference in term of computational costs and disk storage. A schematic comparison between the coupling procedures is shown in Figure 4. For RANS-S.M. model, the RANS calculations of the intake have been performed on the same mesh used in the URANS-URANS calculation. Intake model is coupled with the single passage representation of the fan. A comparison of the computational grids used for the fan domain in the two different coupling approaches is shown in Figures 3. URANS calculations have been performed on 256 cores, 128 cores have been allocated to the intake and 128 cores have been allocated to the fan blades. Unsteady convergence has been obtained after 10 fan revolutions and has been reached after $10-12$ days. In the proposed approach the RANS calculation for intake has been performed on 128 cores and the fan model has been performed on 1 core. The convergence of the coupled solution can be reach in 1 or 1.5 days. In the RANS-S.M. coupling a single solution of S.M. which is used to determine the boundary conditions for the intake RANS including 5 harmonics is reached in $5-6$ minutes.

All the CFD computations have been carried out using the solver reported in di Mare et al. [24] and Wang et al. [25]. The solver has been validated in Carnevale et al. [26]. The solver uses a cell-centred, unstructured, finite volume scheme. The inviscid fluxes are based on Total Variation Diminishing (TVD) variable extrapolation. The gradients are evaluated using weighted least square and the numerical fluxes are evaluated using Roe's (1981) flux vector difference splitting. Van Leer's flux vector splitting [27], and several implementations of Liou-Steffen (AUSM) [28] flux vector splitting are also available. For low Mach number flows, a preconditioning procedure based on the AUSM-UP(+) [29] with Choi-Merkle [30] time derivative preconditioning is employed. Convergence is reached by means of Jacobi iteration or, alternatively with GMRES iterations. The solver is fully implicit, and it is second order accurate in space and in time. Different turbulence closures are available in the code in order to face both high and low Reynolds flow configurations: mixing length, Spalart Allmaras (SA), k-ε, k-ω, and k-ω SST [31]. Low Reynolds correction is applied according the approach proposed in Wilcox [32].

The solver has been optimised to run efficiently on modern multicore and manycore architectures as showed by Hadate [33] [34].

4 Results

The blade considered in the present investigation is representative of a fan mounted on a subsonic civil aero-engine with a pressure ratio range such as: $1.2 \leq \pi \leq 1.6$. Figure 5 shows a comparison of performance maps obtained with the similarity model and with the CFD code presented in the previous section. The CFD computations are steady state, single passage computations with mixing planes. The domain contains an axi-symmetric representation of the intake, operating at 0 incidence, the fan, OGV and ESS. There is an over-estimation of the predicted mass flow-rate by the similarity model due to the fact that the model neglects the blockage due the boundary layer. The difference in prediction of the efficiency is due to the different dissipation of the flux reconstruction. The advantage of the P-G scheme corresponds to a reduction of the numerical dissipation which corresponds to a reduced loss prediction compared to the usual 2^{nd} order MUSCL scheme. All results related to the fan similarity model shown in the rest of the paper have been obtained employing the P-G scheme.

In Figure 6-a and Figure 6-b we compare the C_p distribution at 90% and 50% span. The proposed approach is able to predict the shock location, which is captured within 2 or 3 cells. It can be concluded that the similarity model is able to represent with good accuracy the salient features of the flow field within the passages of a transonic fan. In particular, the model generates the correct entropy rise across the shock system and a creditable approximation of the pressure rise characteristic. The fan similarity model is now applied to the solution of the interaction problem. Previous work has shown that the fan has the effect to mitigate the distortion at fan face with respect to an aspirated intake operating at the same conditions. The inlet distortion level can be represented by a single distortion coefficient, DC_{60}, defined as follow:

$$DC_{60} = \frac{P_0 - P_{0,60}}{q} \tag{8}$$

where P_0 and $P_{0,60}$ are, respectively, the area-averaged total pressure on the fan inlet surface and the average on the 60-degree segment with the lowest mean total pressure. The term q is the dynamic pressure.

Values of DC_{60} as function of intake incidence are shown in Figure 7. The angle $\alpha = 0$ represents the maximum incidence where there is no separation. The reference data are measured on an air intake operated in aspirated configuration. The data are compared to computations for both the aspirated and powered configuration. RANS simulations performed on aspirated configuration properly predict the angle at which the lower lip on the intake begins to separate. Moreover,the calculations reproduce the distortion coefficient DC_{60} at fan face. The powered configuration includes both the intake at incidence and the full annulus fan stage at 97% speed. The simulations confirm the beneficial effect of the presence of the fan in reducing distortions at the fan face and increasing margin of lip stall whith respect to the incidence conditions. The calculations related to the powered configurations are performed using a fully three-dimensional URANS (caption URANS-URANS in Figure 4) model as well as the fan similarity model presented in this paper (caption RANS-S.M in Figure 4). It can be seen that the computations of the powered configuration using the similarity model agree well with the URANS-URANS computations. The labels A and B in Figure 7 represent, respectively, the condition at low distortion and the condition at high distortion, and will be more detailed respect to the different coupling procedure presented in this work. The distortion coefficient DC_{60} measures the overall level of distortion in the flow presented to the fan face. A more detailed comparison of the total pressure field entering the fan is shown in Figure 8. The model RANS-S.M. is able to reproduce the angle where the distortion is triggered in the power configuration. DC_{60} value agree with the CFD data, and the most challenging calculation (CASE B) the RANS-S.M. disagrees with the URANS-URANS calculation for less than 5%. The results provided by the new coupling procedure slightly underestimates the URANS-URANS predictions. This is due to the higher pressure ratio provided by a lower entropy production within the passage due to neglecting the boundary layer. The data in Figure 8 shows that not only does the similarity model reproduce accurately the overall distortion level of URANS calculations, but also it is able to catch the general distribution of total pressure at the fan face. Figure 9 shows a comparison of the isentropic Mach number distribution along the bottom surface of the intake duct. The effect of the fan on the pressure distribution is immediately evident from the comparison of the data for the aspirated intake and the data for the powered intake. In particular, it can be seen that the action of the fan is to lower the static pressure at the fan face in the lower part of the intake and therefore to alleviate the adverse pressure gradient acting on the flow in the diffuser section of the intake. The fan similarity model relies on a Fourier series to represent the flow distortions entering the fan set. The computational cost of the model, whilst much smaller than the cost of a URANS model, is still a function of the number N_k of harmonics needed to represent the distorted flow. The convergence of the model prediction for the static pressure field ahead of the fan is shown in Figure 10. Static pressure profiles at 90% span obtained

with values of N_k from 2 to 4 are compared from reference data extracted from the URANS-URANS calculations. The comparison is performed for both cases A ($\alpha = 1^\circ$) and B ($\alpha = 5^\circ$). It can be seen that for the low incidence case three harmonics are sufficient to reproduce the variation of the static pressure at fan inlet. For the higher incidence case, sharper features are present, corresponding to the separation core at the bottom of the intake, but the shape and values of the static pressure field are still captured satisfactorily with 4 harmonics. Figure 11 and Figure 12 show the variation of static pressure coefficient at fan face at several fractions of the spanwise locations. It can be seen that the similarity model is a better approximation of the URANS flow at higher span levels than at lower span levels. The reason for this is that the approximations used in the similarity model hold better near the fan tip, where the sections are less cambered, the Mach numbers are higher and turning is lower. The disagreement among the RANS-S.M. model and the fully URANS-URANS simulation does not overcome the $5\% - 7\%$ in the worst condition represented by the higher incidence (CASE B) and the lower radial span sections. A specific capability of the present model is the ability to approximate unsteady pressure coefficients on the blade surfaces. This allows the present model to be used as a tool to assess distortion patterns without recourse to fully fledged CFD calculations. Approximate amplitudes and phases plots for the low incidence case and for first two harmonics of the 1^{st} and 2^{nd} Engine Order (EO) signal are shown in Figure 13 and Figure 14. It can be seen that, despite the simplifications introduced in the model, the overall amplitude levels, as well as the shape of the phase relations along the blade surface are well approximated.

5 CONCLUSION

This paper has presented a fan model based on transonic similarity for the calculation of fan-intake interaction problems. The model is based on the approximation of lightly cambered thin sections for the fan and on the assumption that the flow direction departs close to the direction of the section camber line. This approximation gives rise to a transonic similarity law that can be solved for an approximation of the steady state flow in the fan passages. Furthermore, the model can be linearised in the frequency domain to obtain an approximation of the unsteady flow in the fan. The fan interaction problem is therefore reduced to a steady-state computation for the intake and to a steady state and a number N_k of frequency domain computations for the fan set. Each computation for the fan set takes place on a computational domain containing a coarse grid and spanning a single passage. This represents a reduction of computational costs in terms of required core hours and storage. Removing the necessity of the storing the time-solutions implies a considerable reduction of data storage. Furthermore this also leads to faster turn-around time for the post-processing stage.

The model is applied to well-documented case and validated against URANS simulations. It is found that the model reproduces accurately the effect of the fan in terms of DC_{60}, fan inlet total and static pressure field and even the unsteady pressure field in the fan passages. The difference in DC_{60} between the RANS-S.M. coupled model with URANS-URANS is less then 2% for the case with low distortion and less then 5% for the higher incidence condition where an higher distortion is present. Furthermore, the model is able to produce creditable approximations for the unsteady flow inside the fan passage, as shown by the comparison of the model predictions with full URANS simulations for the unsteady pressure amplitude and phase on the blade surfaces.

6 Acknowledgements

The authors gratefully acknowledge Rolls-Royce plc. for funding this work and granting permission for its publication.

REFERENCES

[1] Peters, A., Spakovszky, Z. S., Lord, W. K., and Rose, B., 2015. "Ultrashort nacelles for low fan pressure ratio propulsors". *Journal of Turbomachinery,* ***137***(2), p. 021001.

[2] Hodder, B., 1981. "An investigation of engine influence on inlet performance.[conducted in the ames 40-by 80-foot wind tunnel]".

[3] Larkin, M. J., and Schweiger, P. S., 1992. "Ultra high bypass nacelle aerodynamics inlet flow-through high angle of attack distortion test".

[4] Boldman, D. R., Iek, C., Hwang, D., Larkin, M., and Schweiger, P., 1993. "Effect of a rotating propeller on the separation angle of attack and distortion in ducted propeller inlets".

[5] Carnevale, M., Wang, F., Green, J., and Mare, L. D., 2015. "Lip stall suppression in powered intakes". *Journal of Propulsion and Power,* ***32***(1), pp. 161–170.

[6] Cao, T., Vadlamani, N. R., Tucker, P. G., Smith, A. R., Slaby, M., and Sheaf, C. T., 2017. "Fan–intake interaction under high incidence". *Journal of Engineering for Gas Turbines and Power,* ***139***(4), p. 041204.

[7] Hawthorne, W., and Horlock, J., 1962. "Actuator disc theory of the incompressible flow in axial compressors". *Proceedings of the Institution of Mechanical Engineers,* ***176***(1), pp. 789–814.

[8] Kaji, S., and Okazaki, T., 1970. "Propagation of sound waves through a blade row: Ii. analysis based on the acceleration potential method". *Journal of Sound and Vibration,* ***11***(3), pp. 355IN1–375.
[9] Hynes, T., 1997. "The simulation of turbomachinery blade rows in asymmetric flow using actuator disks". *Journal of turbomachinery,* ***119***, p. 723.
[10] Longley, J. P., 1997. "Calculating the flowfield behaviour of high-speed multi-stage compressors". In ASME 1997 International Gas Turbine and Aeroengine Congress and Exhibition, American Society of Mechanical Engineers, pp. V001T03A084–V001T03A084.
[11] Marble, F. E., 1964. "Three-dimensional flow in turbomachines". *High Speed Aerodynamics and Jet Propulsion,* ***10***, pp. 83–166.
[12] Gong, Y., Tan, C., Gordon, K., and Greitzer, E., 1998. "A computational model for short wavelength stall inception and development in multi-stage compressors". In ASME 1998 International Gas Turbine and Aeroengine Congress and Exhibition, American Society of Mechanical Engineers, pp. V001T01A114–V001T01A114.
[13] Defoe, J., Narkaj, A., and Spakovszky, Z., 2009. "A novel mpt noise methodology for highly-integrated propulsion systems with inlet flow distortion". In 15th AIAA/CEAS Aeroacoustics Conference (30th AIAA Aeroacoustics Conference), p. 3366.
[14] Thollet, W., Dufour, G., Carbonneau, X., and Blanc, F., 2016. "Assessment of body force methodologies for the analysis of intake-fan aerodynamic interactions". In ASME Turbo Expo 2016: Turbomachinery Technical Conference and Exposition, American Society of Mechanical Engineers, pp. V02CT39A036–V02CT39A036.
[15] Cao, T., Hield, P., and Tucker, P. G., 2016. "Hierarchical immersed boundary method with smeared geometry". In 54th AIAA Aerospace Sciences Meeting, p. 2130.
[16] Pullan, G., and Adamczyk, J., 2016. "Filtering mixing planes for low reduced frequency analysis of turbomachines". In ASME Turbo Expo 2016: Turbomachinery Technical Conference and Exposition, American Society of Mechanical Engineers, pp. V02CT39A044–V02CT39A044.
[17] He, L., and Ning, W., 1998. "Efficient approach for analysis of unsteady viscous flows in turbomachines". *AIAA journal,* ***36***(11), pp. 2005–2012.
[18] Hall, K. C., Thomas, J. P., and Clark, W. S., 2002. "Computation of unsteady nonlinear flows in cascades using a harmonic balance technique". *AIAA journal,* ***40***(5), pp. 879–886.
[19] He, L., 2013. "Special issue on Fourier-based method development and application". *International Journal of Computational Fluid Dynamics,* ***27***(2), p. 51.
[20] Carnevale, M., Wang, F., and di Mare, L., 2017. "Low frequency distortion in civil aero-engine intake". *Journal of Engineering for Gas Turbines and Power,* ***139***(4), p. 041203.
[21] Aris, R., 2012. *Vectors, tensors and the basic equations of fluid mechanics*. Courier Corporation.
[22] Wang, F., and Mare, L., 2016. "Hybrid meshing using constrained delaunay triangulation for viscous flow simulations". *International Journal for Numerical Methods in Engineering,* ***108***(13), pp. 1667–1685.
[23] Wang, F., and Mare, L., 2017. "Mesh generation for turbomachinery blade passage with three-dimensional endwall features". *Journal of Propulsion and Power*.
[24] Di Mare, L., Kulkarni, D. Y., Wang, F., Romanov, A., Ramar, P. R., and Zachariadis, Z. I., 2011. "Virtual gas turbines: Geometry and conceptual description". In ASME 2011 Turbo Expo: Turbine Technical Conference and Exposition, American Society of Mechanical Engineers, pp. 347–358.
[25] Wang, F., Carnevale, M., Lu, G., di Mare, L., and Kulkarni, D., 2016. "Virtual gas turbine: Pre-processing and numerical simulations". In ASME Turbo Expo 2016: Turbomachinery Technical Conference and Exposition, American Society of Mechanical Engineers, pp. V001T01A009–V001T01A009.
[26] Carnevale, M., Green, J. S., and Di Mare, L., 2014. "Numerical studies into intake flow for fan forcing assessment". In ASME Turbo Expo 2014: Turbine Technical Conference and Exposition, American Society of Mechanical Engineers, pp. V01AT01A019–V01AT01A019.
[27] Van Leer, B., 1997. "Flux-vector splitting for the euler equation". In *Upwind and High-Resolution Schemes*. Springer, pp. 80–89.
[28] Liou, M.-S., and Steffen Jr, C. J., 1991. "A new flux splitting scheme".
[29] Liou, M.-S., 1996. "A sequel to ausm: Ausm+". *Journal of computational Physics,* ***129***(2), pp. 364–382.
[30] Choi, Y.-H., and Merkle, C. L., 1993. "The application of preconditioning in viscous flows". *Journal of Computational Physics,* ***105***(2), pp. 207–223.
[31] Menter, F. R., 1994. "Two-equation eddy-viscosity turbulence models for engineering applications". *AIAA journal,* ***32***(8), pp. 1598–1605.
[32] Wilcox, D. C., 1988. "Reassessment of the scale-determining equation for advanced turbulence models". *AIAA journal,* ***26***(11), pp. 1299–1310.
[33] Hadade, I., and Mare, L., 2014. "Exploiting simd and thread-level parallelism in multiblock cfd". In Proceedings of the 29th

International Conference on Supercomputing - Volume 8488, ISC 2014, Springer-Verlag New York, Inc., pp. 410–419.

[34] Hadade, I., and di Mare, L., 2016. "Modern multicore and manycore architectures: Modelling, optimisation and benchmarking a multiblock cfd code". *Computer Physics Communications,* ***205***, pp. 32 – 47.

7 Figure

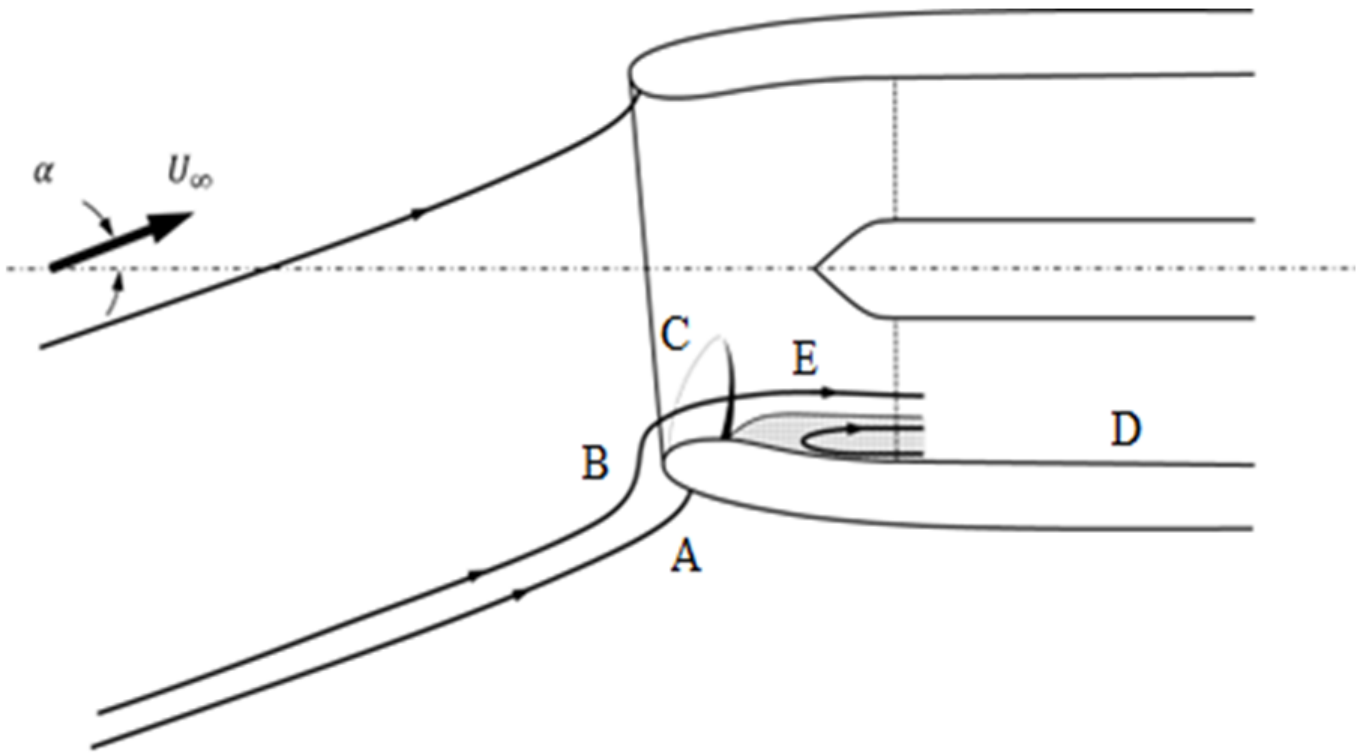

FIGURE 1: Flow arrangement in an intake operating at high incidence.

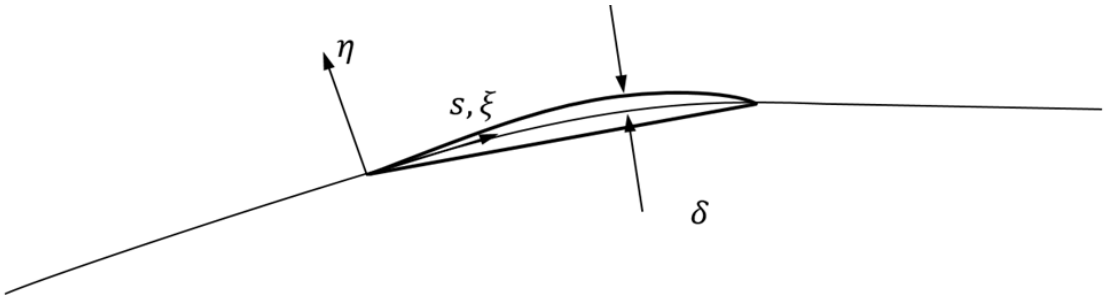

FIGURE 2: Curvilinear coordinate system along the blade streamlines.

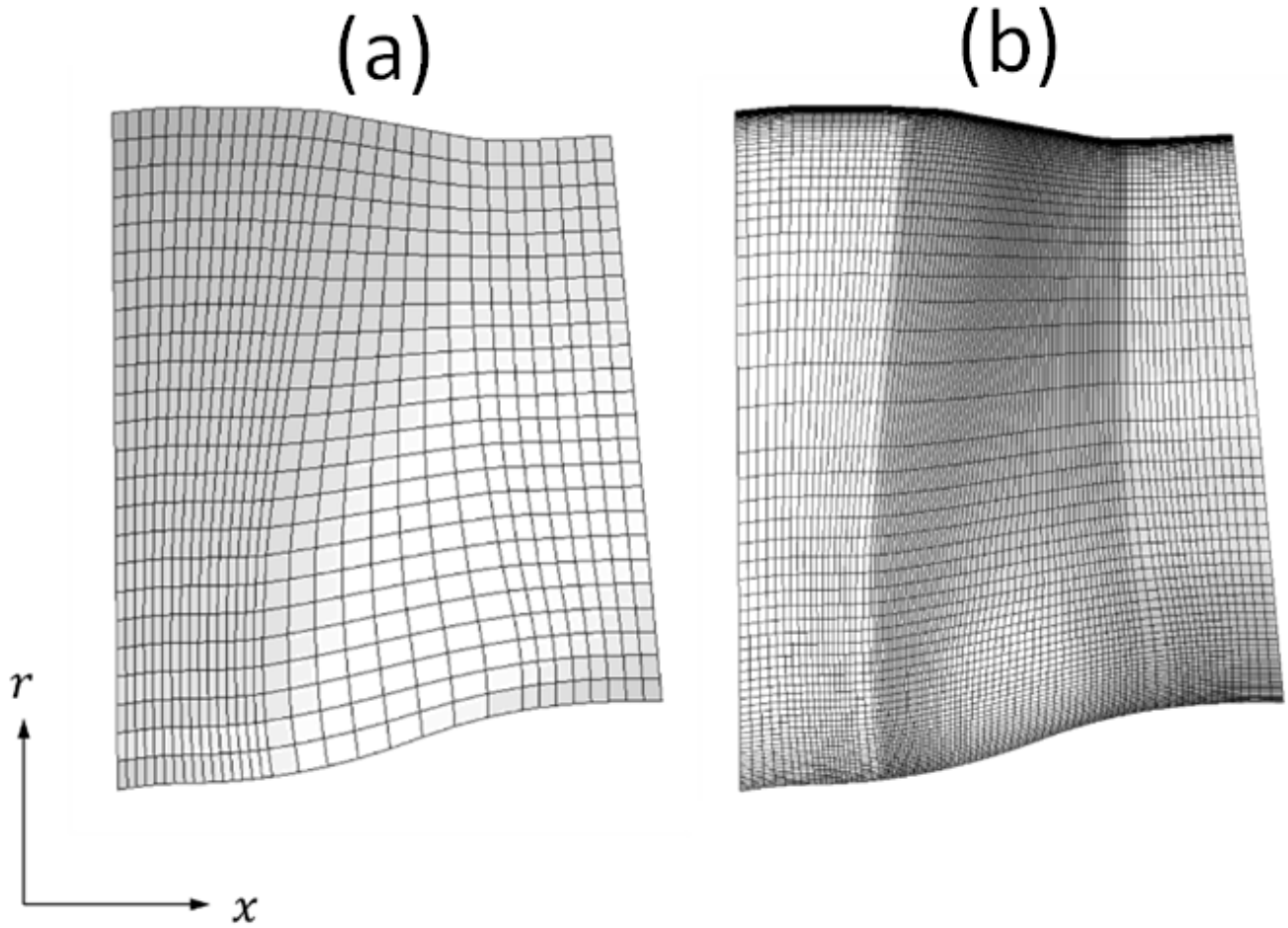

FIGURE 3: Meridional view of the computational grids for fan passage: a) Similarity model b) URANS.

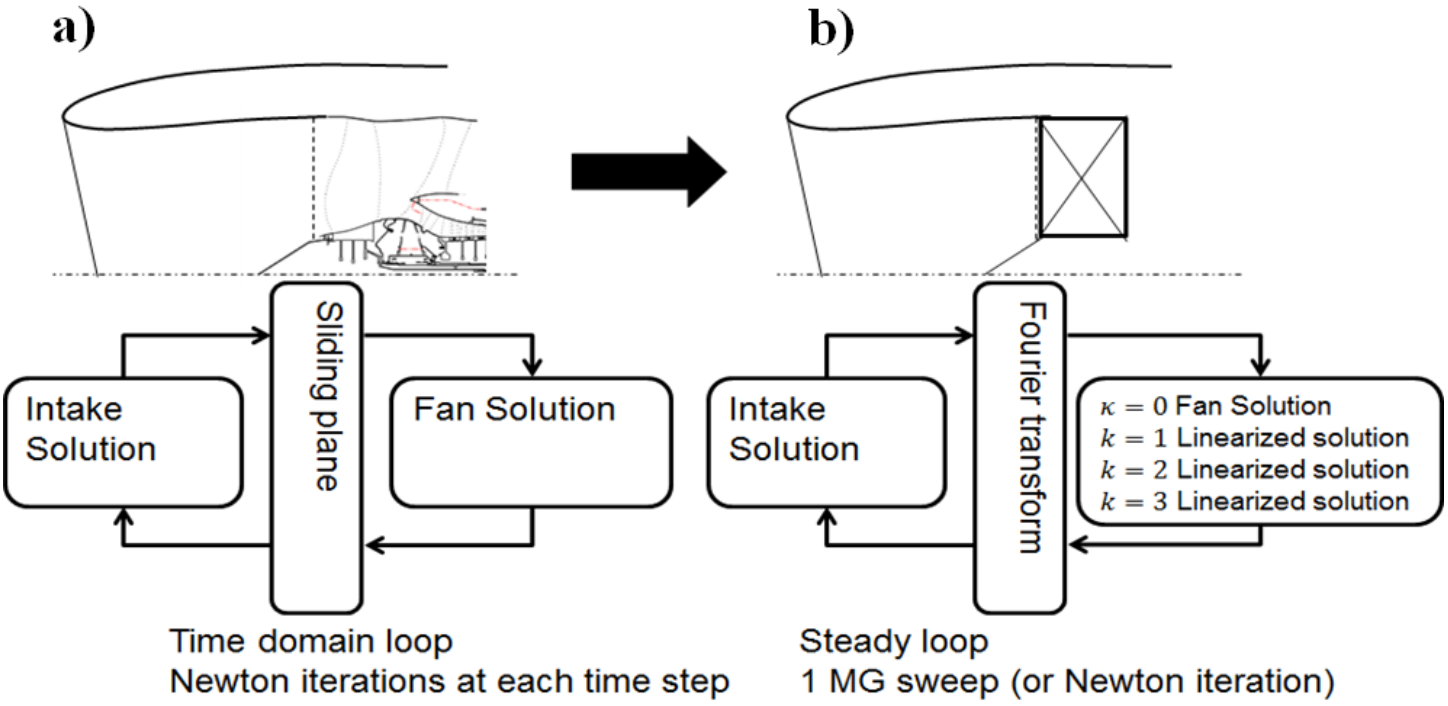

FIGURE 4: a) URANS-URANS; b) RANS-S.M.

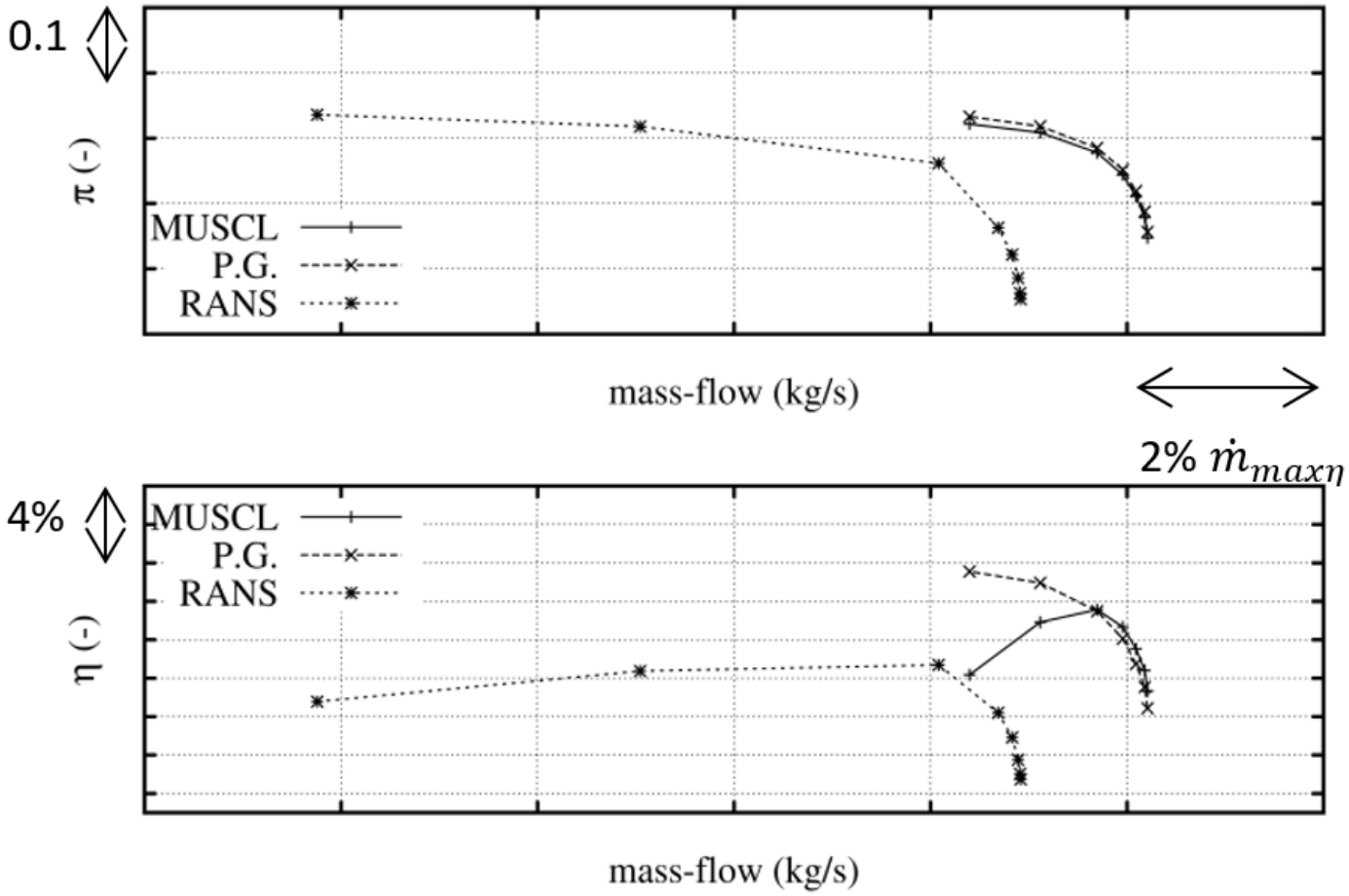

FIGURE 5: Comparison of fan performance predictions from RANS and from the similarity model.

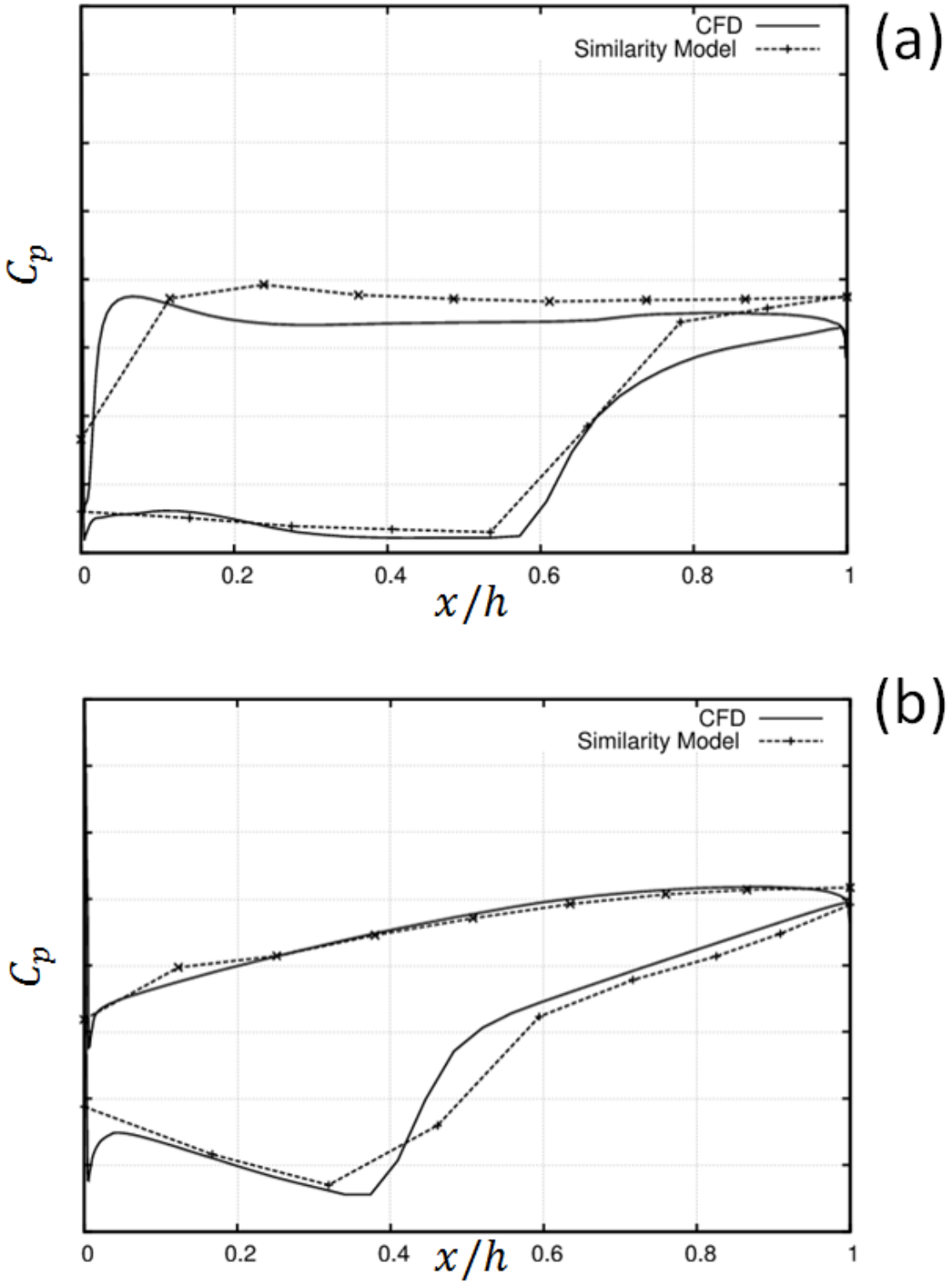

FIGURE 6: a) Comparison of C_p distribution at 90%; b) Comparison of C_p distribution at 50%.

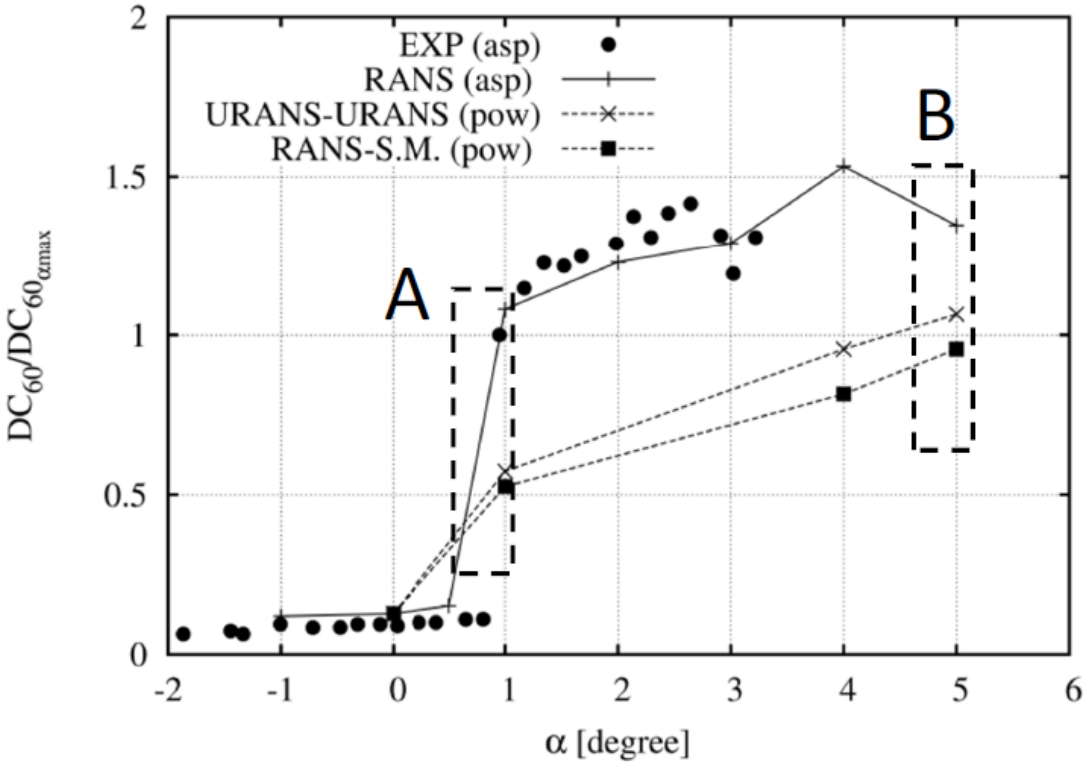

FIGURE 7: Normalized DC_{60} as a function of incidence for an air intake operating in aspirated and powered configuration.

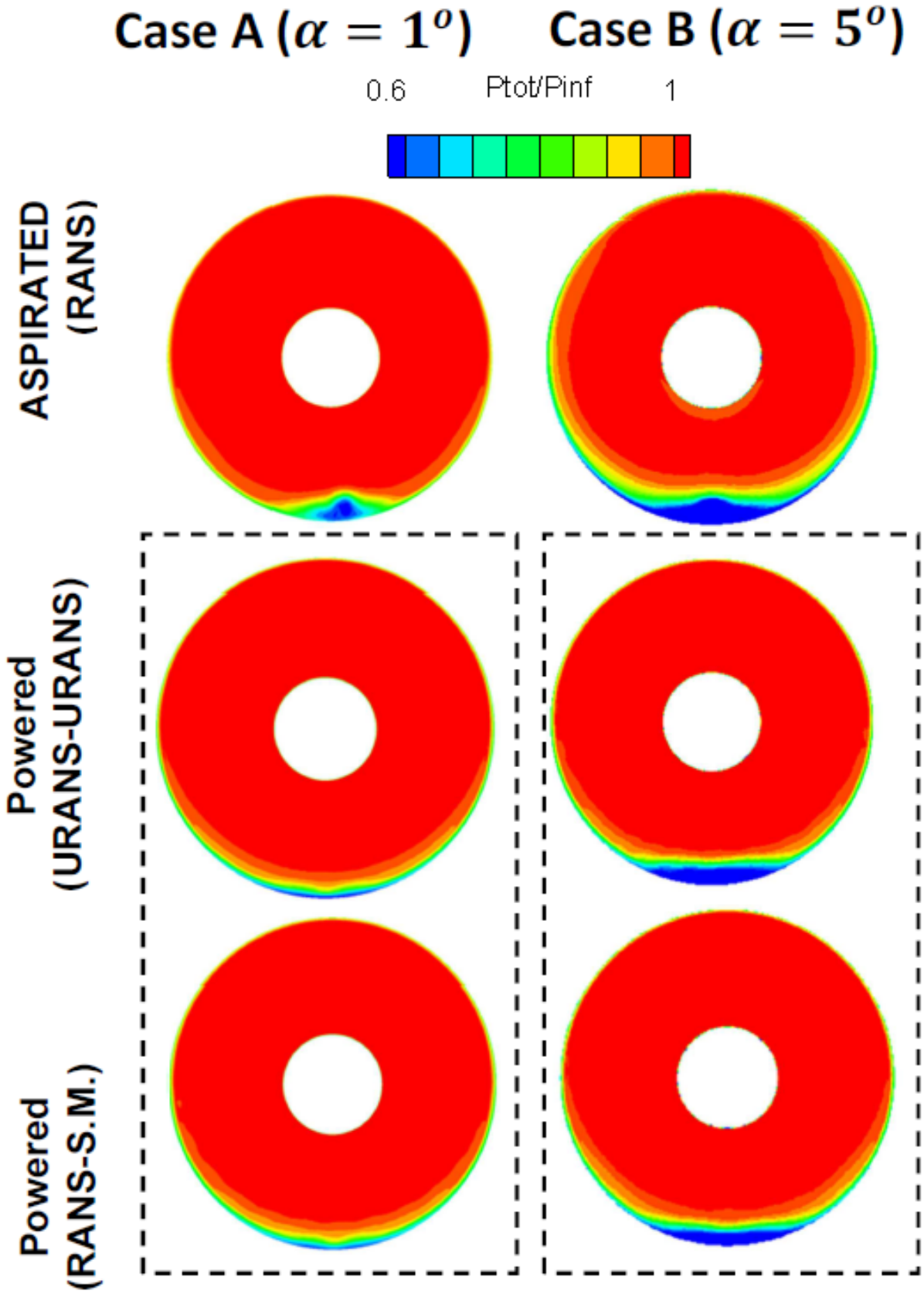

FIGURE 8: Total pressure distribution at fan face for low and high incidence case.

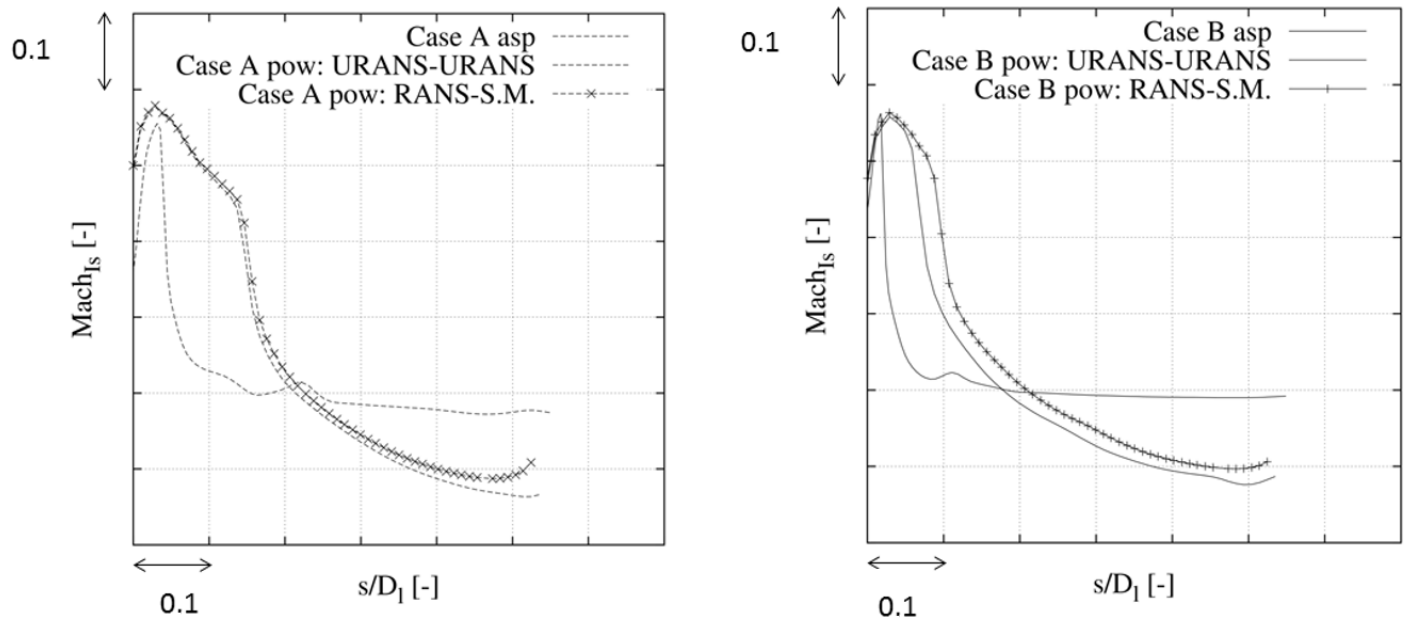

FIGURE 9: Isentroic Mach number on the centre line at the bottom wall of the intake.

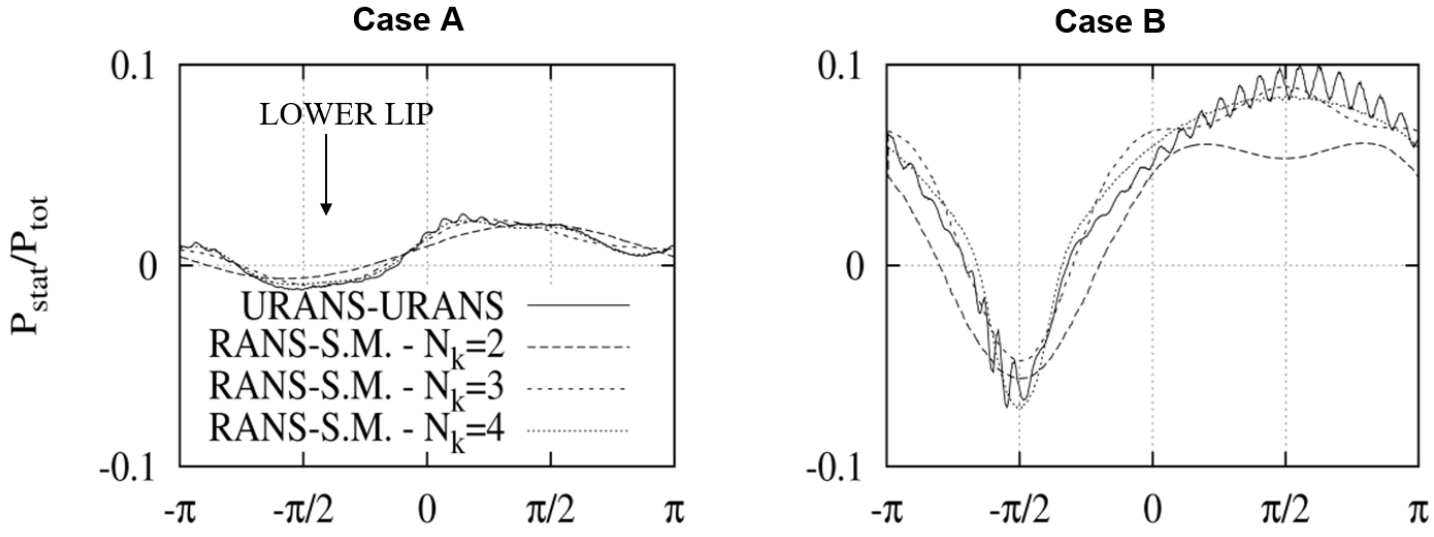

FIGURE 10: Convergence of the Fourier series for the static pressure coefficients at fan face; a) Case A : lower incidence; b) Case B: higher incidence.

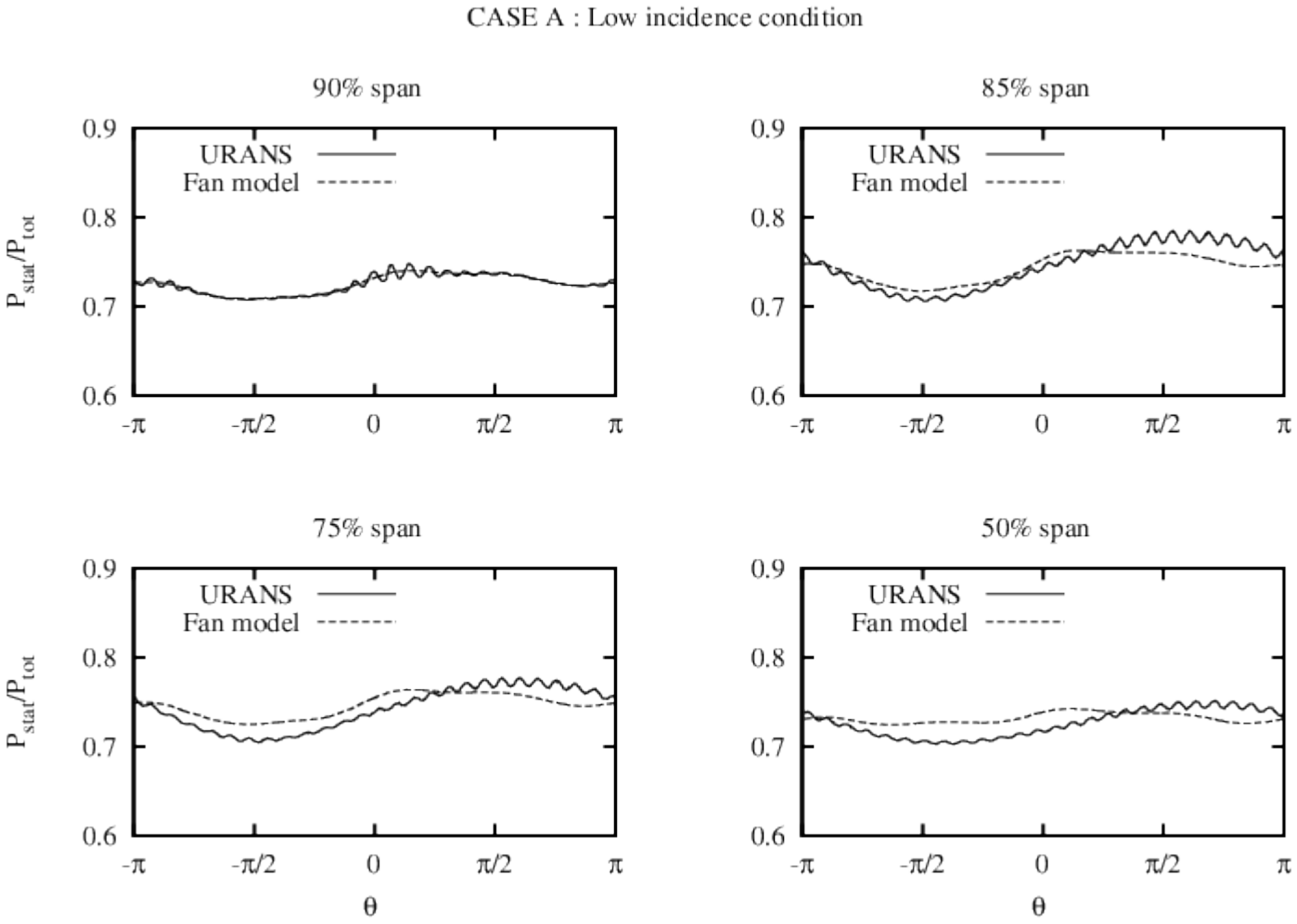

FIGURE 11: Static pressure coefficient at fan face at several levels of span. Low incidence case A ($\alpha = 1°$).

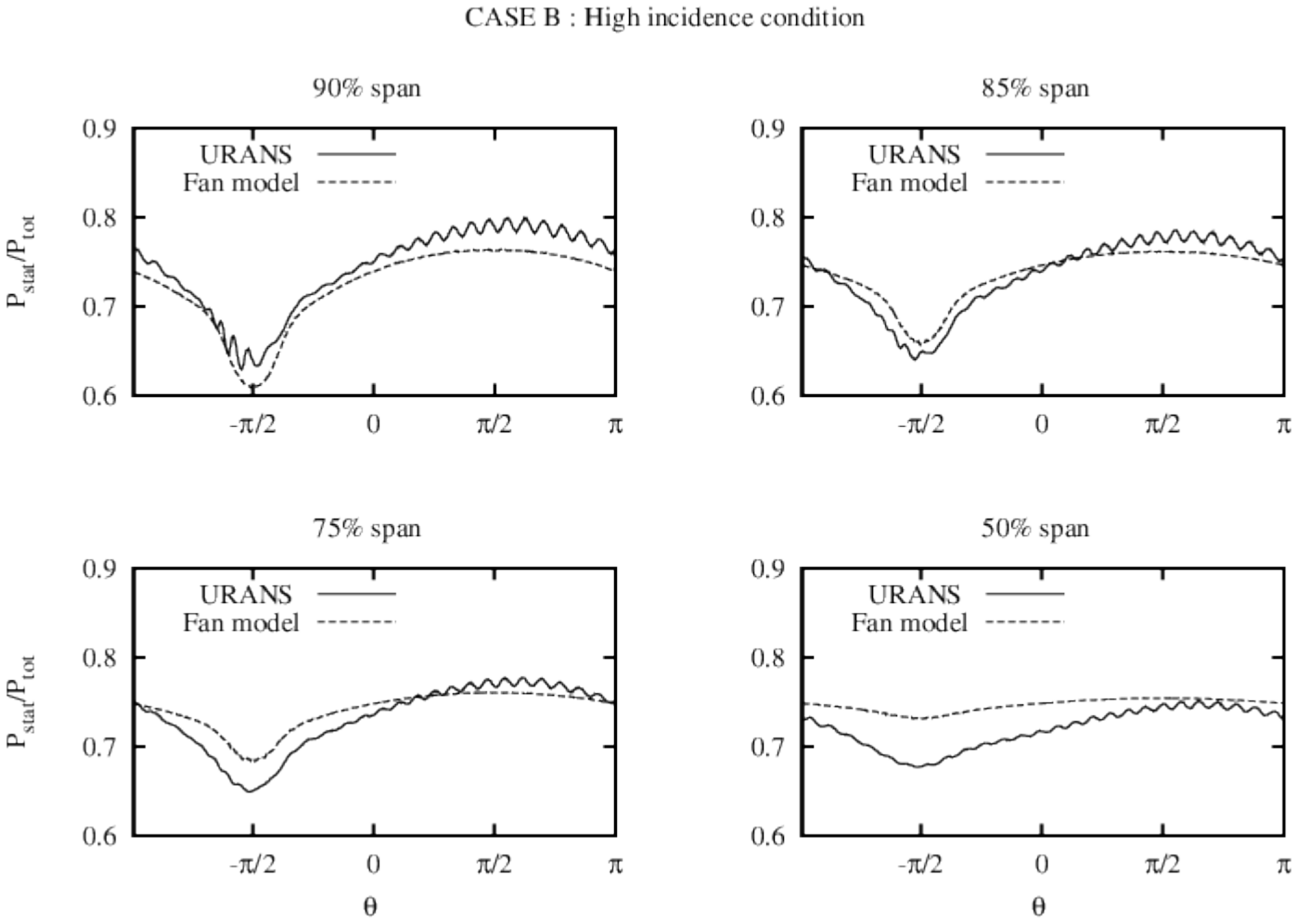

FIGURE 12: Static pressure coefficient at fan face at several levels of span. High incidence case B ($\alpha = 5°$)/

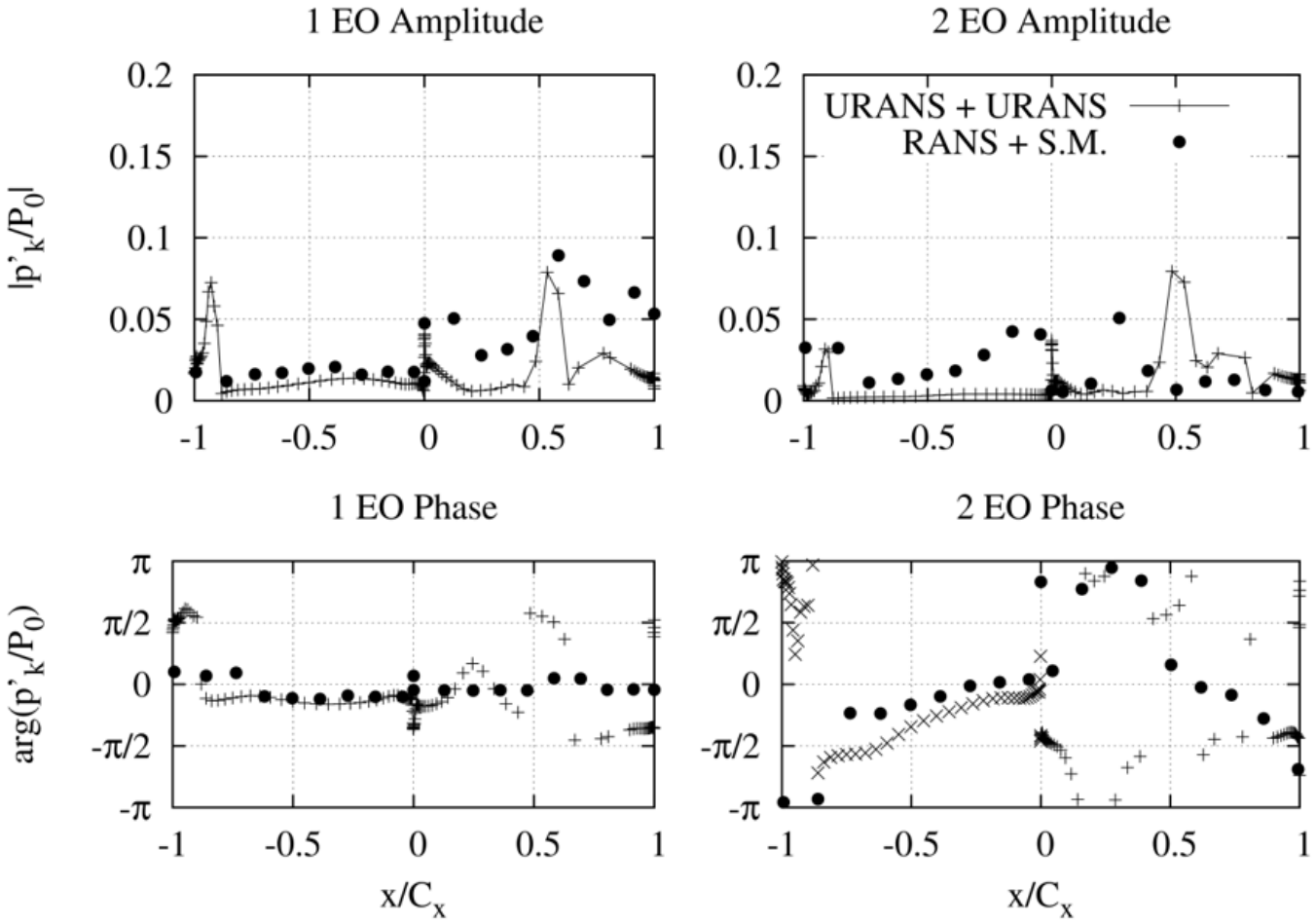

FIGURE 13: Amplitude (top) and phase (bottom) of the unsteady pressure on the blade surface for 1ND disturbances, 90% span. Low incidence case A ($\alpha = 1°$).

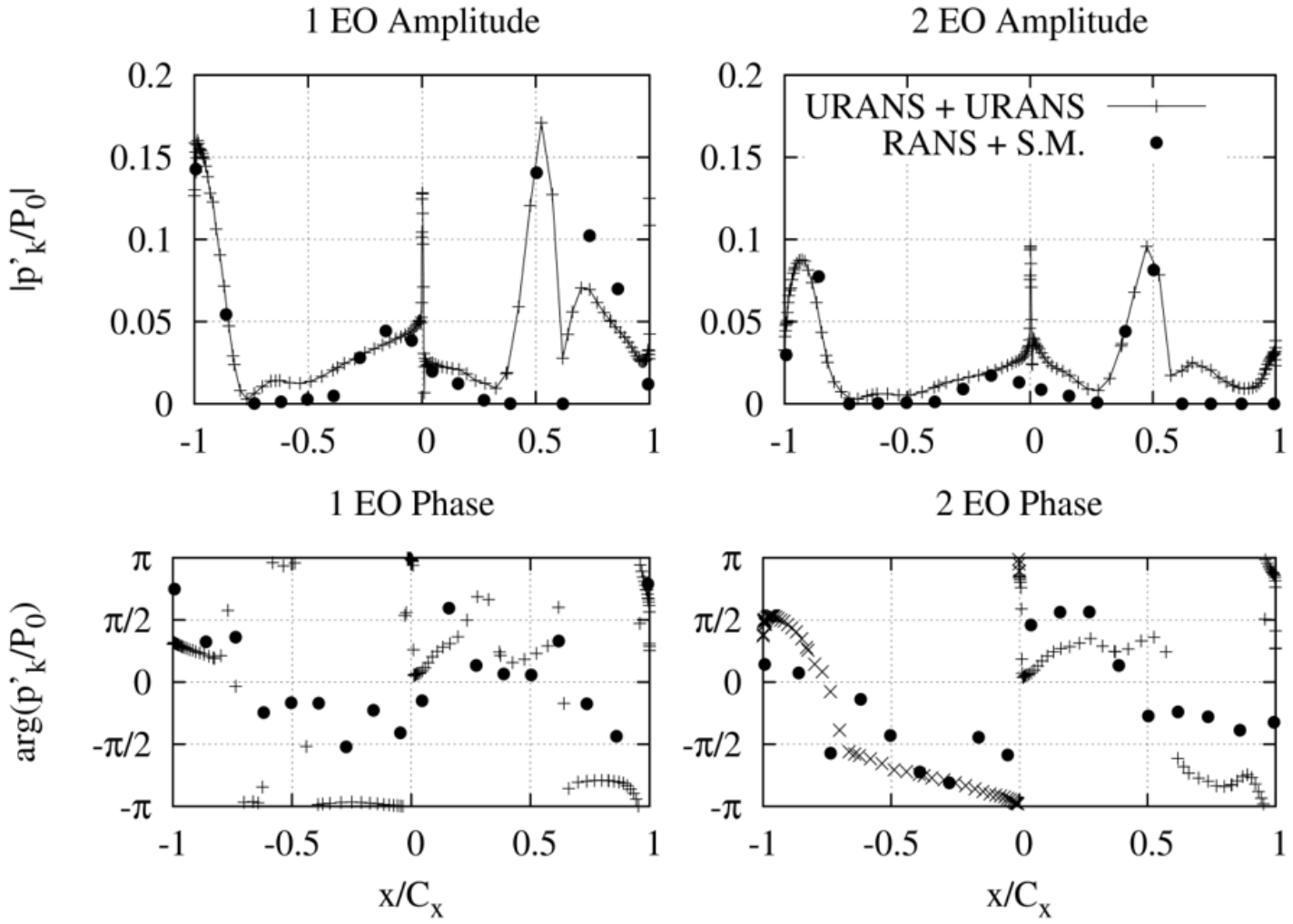

FIGURE 14: Amplitude (top) and phase (bottom) of the unsteady pressure on the blade surface for 1ND disturbances, 90% span. High incidence case B ($\alpha = 5°$).